Molecular Microbiology (2013) 87(2), 338–347 ■
doi:10.1111/mmi.12098
First published online 10 December 2012

Quantification of flagellar motor stator dynamics through *in vivo* proton-motive force control

Murray J. Tipping,[1] Bradley C. Steel,[2] Nicolas J. Delalez,[2] Richard M. Berry[2] and Judith P. Armitage[1]*

[1]*Department of Biochemistry, University of Oxford, South Parks Road, Oxford OX1 3QU, UK.*
[2]*Clarendon Laboratory, Department of Physics, University of Oxford, Parks Road, Oxford OX1 3PU, UK.*

Summary

The bacterial flagellar motor, one of the few rotary motors in nature, produces torque to drive the flagellar filament by ion translocation through membrane-bound stator complexes. We used the light-driven proton pump proteorhodopsin (pR) to control the proton-motive force (PMF) *in vivo* by illumination. pR excitation was shown to be sufficient to replace native PMF generation, and when excited in cells with intact native PMF generation systems increased motor speed beyond the physiological norm. We characterized the effects of rapid *in vivo* PMF changes on the flagellar motor. Transient PMF disruption events from loss of illumination caused motors to stop, with rapid recovery of their previous rotation rate after return of illumination. However, extended periods of PMF loss led to stepwise increases in rotation rate upon PMF return as stators returned to the motor. The rate constant for stator binding to a putative single binding site on the motor was calculated to be 0.06 s^{-1}. Using GFP-tagged MotB stator proteins, we found that transient PMF disruption leads to reversible stator diffusion away from the flagellar motor, showing that PMF presence is necessary for continued motor integrity, and calculated a stator dissociation rate of 0.038 s^{-1}.

Introduction

The bacterial flagellar motor is one of the few rotary motors found in nature and a canonical example of a complex biological nanomachine, being the product of the coordinated expression of over 50 different genes (Macnab, 2003). In *Escherichia coli*, the motor drives rotation of a flagellar apparatus spanning the inner and outer membranes, ultimately turning a long helical filament that propels the swimming cell.

Flagellar motors are driven by ion-motive forces (IMFs): the *E. coli* motor, among others, uses a proton-motive force (PMF) (Manson *et al.*, 1977), while motors in species such as *Vibrio alginolyticus* make use of a sodium-motive force (SMF) (Chernyak *et al.*, 1983). Motor torque is generated by ion flow through several membrane-bound stator units associated with the rotary core of the motor. Individual *E. coli* stator units comprise a stable complex of four MotA and two MotB proteins (Kojima and Blair, 2003), which together are believed to form two stable channels for proton transit (Braun *et al.*, 1999). Ion flow is thought to cause a conformational change in these stators, which is converted to rotary motion by changes in electrostatic interactions between MotA and the rotor protein FliG (Zhou *et al.*, 1998). Details of the exact mechanism of torque generation are still unclear, but torque generation has been shown to be dependent on a crucial aspartate residue in the MotB transmembrane domain (Asp32 in *E. coli* MotB) (Sharp *et al.*, 1995). The protonation state of this Asp residue has also been implicated in stator binding to the flagellar motor in both *Salmonella* and *Vibrio* (Kojima *et al.*, 2009; 2011).

The discrete nature of the torque-generating unit has been demonstrated in a series of 'resurrection' experiments. Complementation of *ΔmotAmotB* mutants by induced expression from plasmids (Block and Berg, 1984; Blair and Berg, 1988) results in recovery of motor speed in stepwise increments in a process called 'resurrection'. Using this method, the maximum number of stators capable of fitting around a motor was determined to be at least 11 (Reid *et al.*, 2006), a figure which agrees with freeze-fracture electron microscopy data (Khan *et al.*, 1988). Resurrection behaviour is also observed in filamentous cells powered by external voltage sources, after disruption and restoration of membrane potential (Fung and Berg, 1995), and in 'chimeric' sodium-driven motors after changes in external Na^+ concentration(Sowa *et al.*, 2005). Stators have thus been shown to individually activate and deactivate in an IMF-dependent fashion.

Accepted 12 November, 2012. *For correspondence. E-mail judith.armitage@bioch.ox.ac.uk; Tel. (+44) (0)1865 613293; Fax (+44) 1865613338. Author contributions: M. J. T., R. M. B. and J. P. A. designed research; M. J. T. performed research; B. C. S., N. J. D. and R. M. B. developed apparatus and analytic tools; M. J. T., B. C. S. and R. M. B. analysed data; and M. J. T. wrote the paper.

Once incorporated, stator units are not permanently fixed in place around the motor. Instead, they appear to transiently engage and disengage with the motor, constantly exchanging with a membrane 'pool' of unbound stators. GFP-tagged MotB molecules incorporated into functioning stators were shown to spend an average of ~ 30 s bound to the motor (Leake *et al.*, 2006). The cause of stator dissociation from functioning motors is currently unknown, and currently published data are inconclusive on the question of whether IMF disruption causes stator dissociation. Fluorescently-tagged stators were shown not to localize to cell poles after SMF disruption in *V. alginolyticus* (Fukuoka *et al.*, 2009), but GFP-tagged MotB molecules were still shown to form discrete spots following PMF disruption in *Salmonella* (Morimoto *et al.*, 2010).

In this study we use, among other techniques, a PMF generated by proteorhodopsin (pR) to power wild-type *E. coli* flagellar motors *in vivo*. Discovered relatively recently, pR is a light-driven proton pump originally found in Pacific marine bacteria (Béjà *et al.*, 2000), and has since been identified in marine bacterial populations worldwide (Sabehi *et al.*, 2003). Unlike its homologues such as bacteriorhodopsin, pR has been shown to be capable of generating a PMF when expressed and excited in *E. coli* cells (Walter *et al.*, 2007). In that study, flagellar motor output (rotation of a tethered cell) was used as a measure of cellular PMF. We have developed this pR-powering technique further to explore the relationship between stator dynamics, motor integrity and the PMF *in vivo*.

This paper characterizes *E. coli* motor response to PMF changes *in vivo*. We use pR both as a tool to augment the PMF generated by the native respiratory apparatus, and as the sole source of *in vivo* PMF. Using back-focal plane (BFP) interferometry to measure motor rotation (Gittes and Schmidt, 1998; Ryu *et al.*, 2000), we show that pR can increase motor speed beyond its physiological norm, and characterize motor behaviour after rapid increases and decreases in PMF. We further determine a timescale for stator disengagement from the motor following PMF disruption, and use data from pR-induced motor resurrections to quantify the binding rate of wild-type stators entering the *E. coli* flagellar motor. Finally, we show by TIRF imaging of functioning, fluorescently labelled stators in tethered cells that stator binding in functioning *E. coli* flagellar motors is PMF dependent, with all stators leaving the motor after it stops following PMF removal.

Results

The effects of pR excitation on motor speed

pR, when expressed in intact *E. coli* cells and excited by illumination, is capable of generating sufficient PMF to drive the flagellar motor (Walter *et al.*, 2007). To test whether this pR-generated PMF could drive the *E. coli* flagellar motor at similar speeds to the native respiratory system, *in vivo* motor speed was measured under several different conditions. We measured motor speed as described previously (Rowe *et al.*, 2003), using 1 μm beads attached to flagellar stubs to monitor rotation. pR was excited with 532 nm laser illumination (see *Experimental procedures*) delivered through the microscope objective. Mean motor speed was measured under five different conditions: (i) wild-type cells, (ii) illuminated wild-type cells, (iii) unilluminated pR-expressing cells, (iv) illuminated, pR-expressing cells and (v) as (iv), but with cells exposed to the respiratory poison sodium azide (30 mM). Figure 1A shows mean motor speeds under these conditions. Mean speeds in conditions (i), (ii), (iii) and (v) were similar (~ 32 Hz in all three cases) indicating that pR could maintain a PMF comparable to the native respiratory system. This PMF could be reversibly disrupted by stopping illumination, resulting in a corresponding motor stop (Fig. 1B). Notably, mean motor speed in illuminated pR-expressing cells not treated with azide was observed to be significantly higher (44 ± 7 Hz) than that of wild-type cells. Figure 1C shows a single example speed/time trace of a motor in a pR-expressing cell subjected to several repeated periods of illumination over 6 min. Motor speed increased in a single large step upon illumination, with the increase essentially complete within the experimental resolution time of 0.1 s.

Time-dependent motor responses to PMF changes

pR-expressing *E. coli* cells were exposed to 30 mM sodium azide solution and illuminated with 532 nm light to maintain the PMF required for motor function. Illumination was then stopped, resulting in motors slowing down to a complete halt. Figure 2A and B shows averaged speed response data, normalized so that initial speed = 1, for two populations of cells: (i) 27 cells where illumination was stopped less than 1 min after addition of azide, and (ii) 24 cells that had been exposed to sodium azide for more than 15 min before stopping illumination. We observed a marked difference between the two populations. Motors in cells exposed to azide for a shorter time took ~ 30 times longer to reach a complete stop after stopping illumination, and there was a high degree of variability between cells. This variability could be attributed to residual native PMF generation caused by incomplete azide inhibition. Motors in cells exposed to azide for extended periods displayed a rapid drop (~ 0.3 s) in speed to ~ 15% of the initial value, followed by a more gradual speed reduction to zero over 1–2 s on average.

We next measured motor recovery on short timescales after transient PMF disruption events. pR-expressing

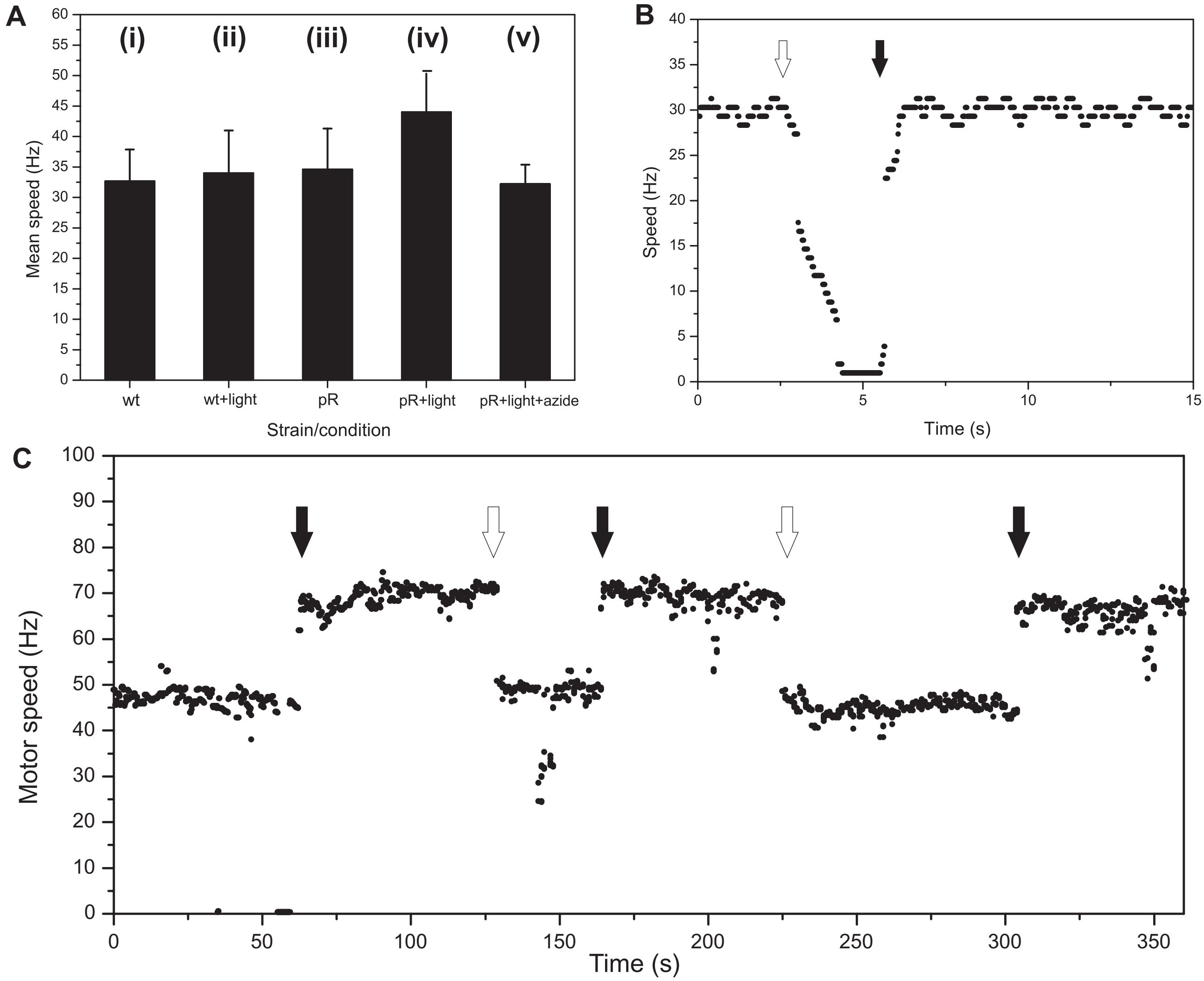

Fig. 1. A. Mean motor speeds of *E. coli* cells under five conditions: (i) wild-type *E. coli*; (ii) wild-type *E. coli,* illuminated by 532 nm laser light; (iii) pR-expressing *E. coli*; (iv) pR-expressing *E. coli*, illuminated with 532 nm laser light; (v) Illuminated pR-expressing *E. coli*, treated with 30 mM sodium azide. Speed increase above wild-type was observed in illuminated pR-expressing cells with intact respiratory systems (iv, those not treated with azide). Motor speed was measured using an adapted *E. coli* motor bead assay. Speed of attached 1 μm polystyrene beads was averaged over 1 min for 50 cells under conditions (i–iv) and 18 cells under condition (v). Error bars show s.d.
B. A representative speed/time graph of a single motor in a pR-expressing *E. coli* cell treated with sodium azide, showing reversible loss of function following PMF disruption upon stopping and resuming illumination.
C. A representative speed/time graph of a single motor in a pR-expressing *E. coli* cell with an intact respiratory system, showing reversible speed increases following illumination.
Arrows in B and C show where illumination was stopped (white) and started (black).

E. coli cells were illuminated with 532 nm light and exposed to azide for 15 min to ensure complete inhibition of the native respiratory chain. Cells were then subjected to repeated short stops in illumination (time without light < 1 s). Rapid speed reductions upon removal of illumination were observed as in Fig. 2B, with motor speed returning to its previous value after re-illumination. Figure 2C shows normalized, averaged speed recovery data for 28 motor speed increase events; a single example can be seen in Fig. S1. Motors did not always stop completely during these short PMF disruptions, consistent with the results shown in Fig. 2B. These averaged data show that after long periods of azide exposure, motor recovery following transient (< 1 s) PMF disruption events is a two-stage process. First, motors increased quickly (within 0.25 s) to around 80% of their initial speed. Subsequent speed recovery to 100% of initial speed took an average of 3 s. This recovery is on a different timescale to the speed increase observed upon illumination in untreated cells (Fig. 1C), where averaging 21 such traces showed that a stable speed was typically reached within 0.2 s (Fig. S2).

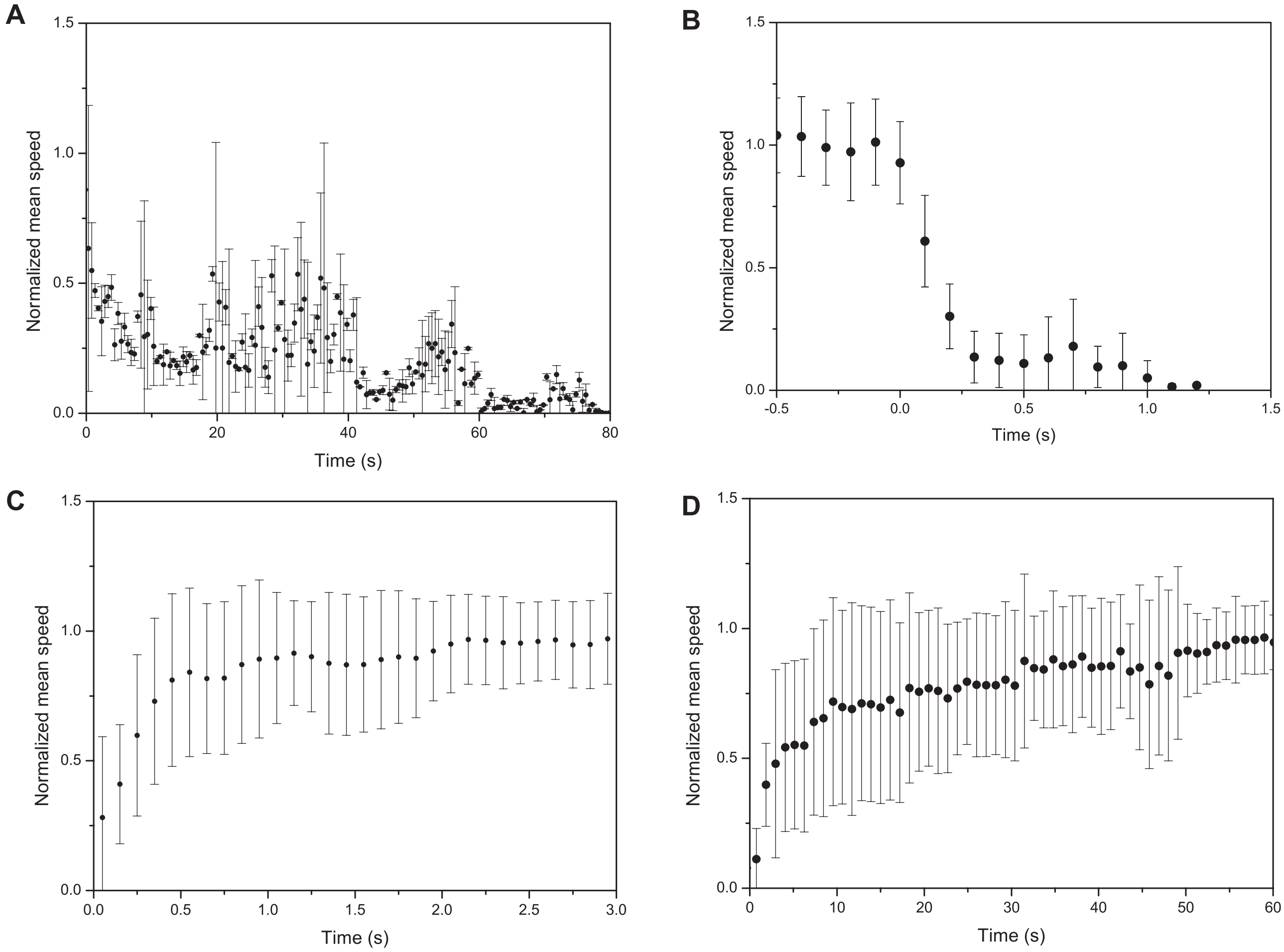

Fig. 2. Mean normalized speed/time graphs after stopping (A, B) or restarting (C, D) illumination. Graphs show responses following: (A) Illumination stop after < 1 min exposure to azide; (B) Illumination stop after > 15 min exposure to azide; (C) Illumination return after < 1 s without illumination; (D) Illumination return after > 20 s without illumination. Data were averaged from 27, 24, 28 and 37 cells in A–D respectively. Individual motor speeds were normalized to the speed observed 1 s before stopping illumination. Error bars show s.d.

We then examined motor response to extended periods of PMF loss. pR-expressing cells were treated with sodium azide and illuminated with 532 nm light to maintain cellular PMF. Stopping illumination caused motors to slow down and reach a complete stop. Cells were then left without illumination for > 20 s. After this time, illumination was restored. Thirty-seven individual traces were normalized as before and averaged (Fig. 2D). Motors in these cells took much longer to recover than those subjected to brief periods of PMF disruption, and often did not return to their maximum speed observed before PMF reduction. Individual motors also displayed larger variation in intermediate speeds during motor speedup than those subjected to transient PMF disruption.

In vivo *motor resurrection after PMF restoration*

We used the PMF control system to investigate motor resurrection after PMF disruption *in vivo*. Twenty-five speed/time traces of motors in cells subjected to zero PMF regimes (for times ranging from 5–80 s) showed clear intermediate steps in motor speed during recovery. Three representative resurrection traces, with histograms of speed levels observed during resurrection, can be seen in Fig. 3. The observation of intermediate speed steps caused by stator activation, rather than a smooth increase, is consistent with previous studies showing motor resurrection after IMF loss (Fung and Berg, 1995); chimeric sodium-driven motors also show this resurrection pattern after disruption and restoration of sodium-motive force (Sowa *et al.*, 2005). To confirm that speed increments were due to activation of individual stators, mean differences between adjacent speed levels in these traces were calculated. Average motor speeds over 1 s windows were calculated and sorted into histograms with 1 Hz bins (Fig. 3, right). Gaussian curves were fitted to histogram peaks; by measuring the distance between neighbouring peaks, mean step size was calculated to be

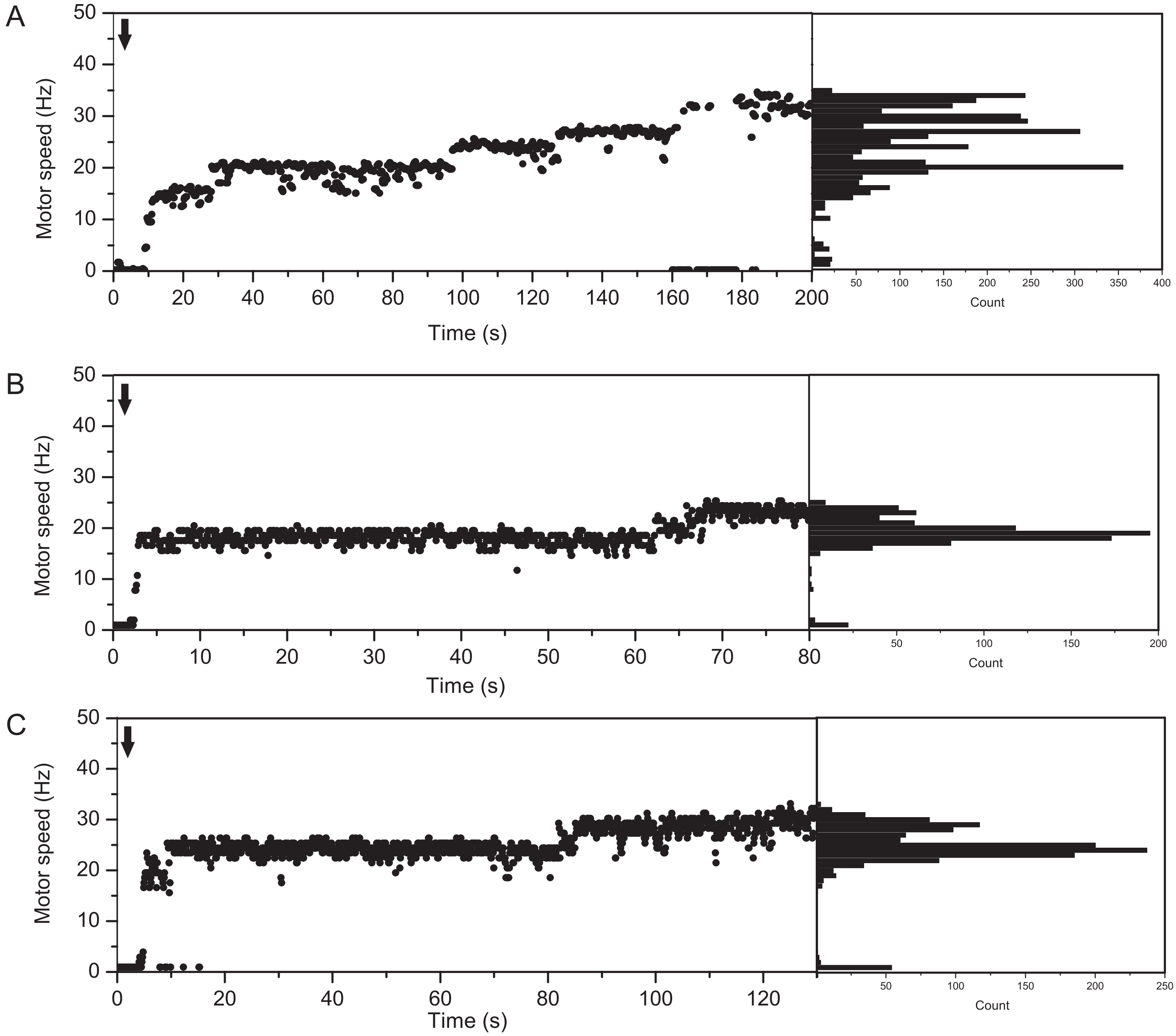

Fig. 3. Speed/time traces and speed histograms for three representative motor resurrection events labelled A, B and C following PMF disruption in pR-expressing *E. coli* cells. Traces of this type were used to calculate a rate constant for stator binding to a single site on the motor of $0.06 \pm 0.03\ s^{-1}$. Arrows show where illumination was restarted. Histograms are of motor speed over successive 1 s intervals in 1 Hz bins after re-illumination.

5.9 ± 1.6 Hz. This figure is similar to that previously calculated for the contribution of individual wild-type stator units (Reid *et al*., 2006). Individual steps in speed during motor resurrection for these 25 traces were then isolated using a step-finding algorithm (Smith, 1998). The average time spent at the final intermediate speed level in each trace was 16.7 ± 8.2 s ($n = 25$). Assuming that the motor could bind no more stators after the last step (i.e. the motor was then 'full'), we obtained a rate constant of $0.06\ s^{-1}$ (error bounds $0.04–0.12\ s^{-1}$) for stator binding to a single free binding site in the motor. In five traces we were also able to measure the time interval before the second-last step, with an average of 11.6 ± 12 s. The simplest model of stator binding, with the limiting factor being the number of available free binding sites, predicts that this interval should be half as long on average as the last interval if it represents the time taken for a stator to bind to either of two free binding sites. Our result is consistent with this model, but the technical difficulty of generating reliable data with many clear resurrection steps prevented us from drawing stronger conclusions.

Resurrection experiments of this type are unable to show whether stators remain attached to the motor following IMF disruption. To determine whether this was the case, we monitored the behaviour of GFP-tagged MotB molecules in functioning motors using TIRF microscopy using

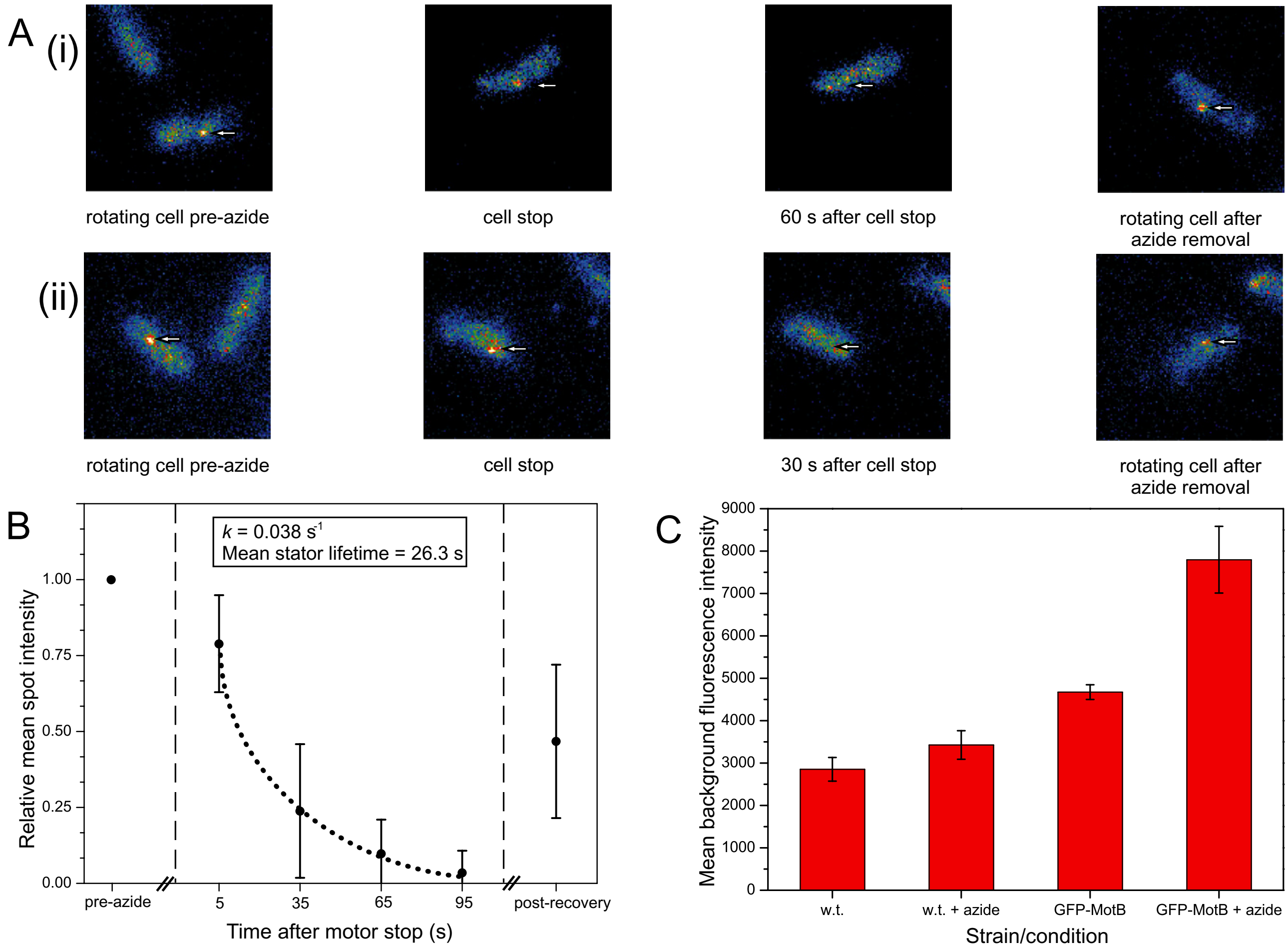

Fig. 4. A. Representative TIRF images of two single, tethered *E. coli* cells expressing GFP-MotB during a azide-induced stator dissociation. Centre of rotation is indicated by the white arrow for each cell. From left to right, images show: GFP-MotB motor spot at the centre of rotation, showing torque-generating stator units bound to the motor before PMF disruption; persistence of motor spot after motor stop, with stators still bound to the stopped motor; complete spot dissipation 30 or 60 s after motor stop; return of motor spot after resumption of rotation, showing return of stators to the flagellar motor following restoration of PMF.
B. Mean motor spot intensity before and after transient PMF disruption in 11 tethered *E. coli* cells. Motors were situated at the centre of rotation for each cell. Individual spot intensity was normalized to the intensity observed prior to azide treatment. A single-exponential decay curve (dotted line) was fitted to the time-course following motor stop (adjusted R-squared value = 0.995). Dissociation rate constant k was calculated to be $0.038 \pm 0.005\ s^{-1}$, corresponding to a mean stator lifetime of 26.3 ± 1.4 s. 'Post-intensity' spot value is taken from the final fluorescence image of each cell following motor recovery.
C. Graph comparing cellular background fluorescence of 25 cells of wild-type and GFP-MotB expressing *E. coli* cells, showing increased membrane fluorescence in GFP-MotB expressing cells following 10 min exposure to azide.

methods similar to those described previously (Leake *et al*., 2006). PMF was reversibly disrupted in *E. coli* cells expressing genomic GFP-MotB by addition and removal of 30 mM sodium azide. pR could not be used in these experiments because of unavoidable spectral overlap between pR and fluorophore excitation wavelengths. Figure 4A shows two representative single-cell examples of the resulting PMF-dependent stator dynamics. Before addition of azide, rotating tethered cells displayed a characteristic GFP-MotB spot at the centre of rotation (Fig. 4A, first images). Addition of azide to the motility medium via a flow cell caused motors to slow down and stop, with mean time from addition of azide to complete motor stop, assessed by brightfield observation of the cell, measured to be 189 ± 79 s ($n = 11$). TIRF imaging of cells as soon as possible (5 ± 1 s) after motor stop revealed persistence of GFP-MotB spots, indicating continued association of stators with the motor basal body (Fig. 4A, second images). TIRF imaging was continued at 30 s intervals after motor stop, showing gradual dissociation and diffusion of GFP-MotB motor spots away from the motor. Figure 4B shows mean motor spot intensity (normalized to the value observed prior to azide treatment) following motor stop. Dissipation of GFP-MotB spots was complete 2 min after motor stop in all observed cells, indicating that stators were no longer bound to the motor after this time

(Fig. 4A, third images). The reduction in spot intensity following motor stop followed a pattern consistent with exponential decay; fitting a single-exponential decay curve to this dataset (adjusted r-squared value: 0.995) allowed us to calculate a stator dissociation constant $k = 0.038 \pm 0.002\ s^{-1}$. This corresponds to a mean stator lifetime following PMF loss of 26.3 ± 1.4 s. Dissociation of stators from the motor into the membrane pool after PMF disruption was further confirmed by observation of an increase in average membrane fluorescence in 25 azide-treated GFP-MotB cells compared with 25 untreated GFP-MotB and 25 wild-type cells (Fig. 4C). No such PMF-dependent dissociation was observed in cells expressing YPet-FliM, which displayed fluorescence spot persistence at the centre of rotation 10 min after exposure to sodium azide (Fig. S3). After complete stator dissociation was observed, azide was removed from the motility medium, allowing cells to recover native PMF generation capability and restore motor rotation. Mean time for motor recovery after removal of azide was measured to be 291 ± 231 s ($n = 11$). This large degree of variation is likely due to differing responses to azide poisoning between individual cells. Motor spot formation following removal of azide was monitored by TIRF imaging of cells at 30 s intervals. All recovered motor spots were in cells that had started rotating again (Fig. 4A, fourth image), indicating close coupling between stator relocalization and recovery of torque generation. Motor spot intensity following recovery was consistently lower than the same spot measured prior to azide poisoning; this may be due to inability of cells to completely recover fully from azide poisoning (perhaps leading to fewer bound stators) or photobleaching of GFP-MotB during monitoring after azide removal.

Discussion

Recent investigations into the relationship between the ion-motive force and *E. coli* flagellar motor integrity and function have used sodium-driven motors because of the relative simplicity of varying SMF across intact cell membranes (Sowa *et al.*, 2005; Lo *et al.*, 2007). The ability to light-power *E. coli* enables the response of the wild-type *E. coli* motor to changes in PMF, and motor resurrection after PMF disruption, to be studied *in vivo*; previously, such experiments were limited to photosynthetic bacteria (Armitage and Evans, 1985). Light-powering also enables IMF changes to be effected on significantly shorter timescales compared with SMF-based approaches.

The response of the motor to differing light levels reveals some of the underlying relationships between motor function and cellular bioenergetics. At high loads, such as those used in these experiments, speed has been shown to be proportional to IMF in both proton and sodium-driven flagellar motors (Gabel and Berg, 2003), (Sowa *et al.*, 2003). Unlike in previous studies (Walter *et al.*, 2007), we observed an increase in rotation rate upon illumination above that previously-measured, suggesting a corresponding increase in physiological PMF. This result is the first observation of *E. coli* motor rotation powered by a PMF higher than the physiological norm, and agrees well with previous observations made with the sodium-driven chimeric flagellar motor, where a linear relationship between motor speed and SMF was observed up to 200 mV (Lo *et al.*, 2007). The short timescale (< 0.1 s) of these steps, and the lack of observed intermediate speed levels, suggest that these increases are purely IMF-driven without the need for any change in motor stoichiometry.

The use of pR to generate a PMF *in vivo* allowed us to monitor motor response to PMF disruption events. Motors were observed to respond to PMF disruption and restoration in a two-stage fashion, with motor speed increasing or decreasing rapidly (with a timescale on the order of milliseconds) before changing more gradually. The lack of observable intermediate steps during these events is a sign that, like the speed increase observed in uninhibited cells, this motor recovery pattern is not due to activation or deactivation of individual stator units. The cause of this two-stage pattern is unknown but may be due to vestigial PMF generation or other bioenergetic effects. However, after extended PMF disruption stepwise resurrection is observed, with motor speed increasing in step sizes similar to the contribution of single stators to motor rotation at the same load (Reid *et al.*, 2006). Our observation of steps in resurrection under these conditions shows that functional stator binding to the rotor in the wild-type *E. coli* motor is PMF-dependent, and that PMF disruption leads to a temporary loss of function in individual stators. Physical dissociation of stators, rather than altered conformation, was confirmed by TIRF imaging of motors before, during and after PMF disruption. This is the first observation of such PMF-dependent stator dissociation in *E. coli,* and contrasts with the apparent absence of stator loss when PMF is disrupted through by ionophore action in *Salmonella* (Morimoto *et al.*, 2010). Such a difference in phenotype may simply be a result of the differing experimental methodologies used in that experiment (e.g. the use of an uncoupler to disrupt PMF). However, it potentially indicates hitherto-unknown differences in stator behaviour between the flagellar motors of *E. coli* and *Salmonella*. Our observation of clear intermediate steps during resurrection allowed us to estimate a rate constant of $0.06 \pm 0.03\ s^{-1}$ for the final stator binding event observed during motor resurrection, while the stator dissociation rate observed using TIRF microscopy following motor stop was estimated to be $0.038 \pm 0.002\ s^{-1}$, in both cases using cells expressing MotB or GFP-MotB at genomic levels. These figures represent two independent quantifications of stator binding and dissociation rates, and are of similar magnitude to the previously-estimated GFP-tagged stator turnover rate of $0.04 \pm 0.02\ s^{-1}$ in functioning motors, where binding rate was posited to equal the rate of dissociation (Leake *et al*., 2006). GFP-MotB spots corresponded closely to motor rotation both upon removal and restoration of PMF. The exponential fit of Fig. 4B predicts 100% spot intensity at about $t = -1$ s, the same time at which rotation stopped within the limits of uncertainty. The simplest explanation would be that PMF falls sharply to zero at this time, triggering motor stopping and stator dissociation. However, the data of Fig. 2A indicate that speed loss, and so PMF loss, after azide addition is gradual rather than sudden. Thus the loss of fluorescence coinciding so closely with motor stop indicates either that stator dissociation only begins at very low PMF, or that it is the loss of rotation rather than loss of PMF that directly triggers stator dissociation. Furthermore, the lack of any measureable delay between motor stop and the onset of stator dissociation indicates that any intermediate state between binding and activation of stators (Li *et al*., 2011; Yonekura *et al*., 2011) must be short lived. Recent work has shown that the switch complex protein FliM undergoes signal-dependent turnover and stoichiometry variation (Delalez *et al*., 2010) (Yuan *et al*., 2012). PMF-induced dissociation was not observed for YPet-FliM, suggesting that rotor dynamics are not directly connected to stator turnover.

In resurrection traces where stepwise speed increases were observed, motors did not always return to their original speed. This difference in motor speed could be due to a difference in cellular PMF before and after PMF disruption, despite illumination levels remaining the same throughout, and rapid illumination changes resulting in return to the original motor speed. Prolonged zero-PMF regimes may irreversibly damage the cell's ability to maintain PMF. Alternatively, after prolonged dark periods when stators will have diffused into the general membrane pool, the limiting factor for motor speed may be the number of functional stators able to bind to the motor, caused by damage to either free stators, bound stators or binding sites at the motor. Further theoretical work into stator dynamics and packing around the motor could provide testable hypotheses for more quantitative studies in this area.

Experimental procedures

Construction of experimental E. coli *strains*

A construct was made, based on plasmid pDS132 (Philippe *et al*., 2004) which replaced the wild-type *fliC* gene of *E. coli* strain RP5232 (Parkinson, 1978) with mutant variant *fliCst* (Kuwajima, 1988) by allelic exchange. This mutant exposes the hydrophobic core of the flagellar filament, improving flagellar binding to hydrophobic surface such as beads or glass. Insertion of mutant *fliCst* into the *E. coli* chromosome was done by allelic exchange as described in (Philippe *et al*., 2004).

Growth of E. coli *cultures*

Escherichia coli were grown aerobically at 30°C with shaking in 5 ml T-broth (10 g l^{-1} bacto-tryptone, 5 g l^{-1} sodium chloride). Cells were harvested at mid-exponential phase (typically OD_{600} 0.6).

In experiments involving light-powered *E. coli* cells, cultures were grown in T-broth plus ampicillin (100 μg ml^{-1}). SAR86 γ-proteorhodopsin (a gift from Jan Liphardt, UC Berkeley) was expressed in strain RP5232-*fliCst* using the pBAD-His C expression system (Invitrogen). Production of proteorhodopsin protein was induced by adding DL-arabinose to a fixed concentration of 1 mM in growth medium when cells reached OD_{600} 0.4; cells were incubated for a further hour after induction at 30°C with shaking to allow protein expression to take place. Along with DL-arabinose, all-trans-retinal (a necessary cofactor) was added to 10 μM in the growth medium. Cells were harvested by gentle centrifugation ($4500 \times g$ for 2 min) and resuspended in *E. coli* motility buffer (10 mM potassium phosphate, 0.1 mM EDTA, pH 7.0).

Measurement of flagellar motor speed

Cells were bound to a glass coverslip with polylysine. 1 μm-sized polystyrene beads were attached to 'sticky' flagellar stubs as described in (Ryu *et al*., 2000). Motor speed was measured by monitoring bead position using back-focal-plane (BFP) interferometry as described in (Rowe *et al*., 2003). A sampling rate of 2.0 KHz was used.

Flagellar motor speeds were determined in all cases from power spectra of combined (*x, y*) data, as described in (Sowa *et al*., 2005). Data windows of 1 s were used, with windows beginning at intervals of 0.1 s. This provided a mean speed resolution of 1 Hz, with a time resolution of 0.1 s.

Light-powering E. coli *cells*

To excite proteorhodopsin, illumination was provided using a 532 nm green laser (Thorlabs). The laser was set up to provide illumination through the microscope objective path, allowing simultaneous bead monitoring. The power density through the coverslip was 5 kW m^{-2}. The light path contained a computer-controlled shutter to enable rapid control of illumination. Cells were observed with a faint red light (0.9 W m^{-2}), to prevent unwanted proteorhodopsin excitation.

In experiments where native respiration was inhibited, the respiratory poison sodium azide was used to effectively suppress the electron transport chain and ATP hydrolysis by ATP synthase (Kobayashi *et al*., 1977). 30 mM of sodium azide solution was passed through the slide containing cells to be examined immediately before the start of analysis.

Fluorescence microscopy

A home-built inverted TIRF microscope was used as described previously (Leake *et al*., 2006) (Leake *et al*., 2008). Excitation wavelengths of 473 and 532 nm were used for GFP and YPet imaging respectively. Fluorescence emission was imaged at 50 nm per pixel in frame-transfer mode at 24 Hz by a 128 × 128-pixel, cooled, back-thinned electron-multiplying charge-coupled device camera (iXon DV860-BI; Andor Technology).

Data processing

Data analysis was done using custom-written scripts in Matlab (Mathworks) and LabView (National Instruments).

For results where many speed-time traces were averaged, individual speed-time traces were first normalized, so that 1 = the median speed over 1 s prior to PMF disruption. Averaged speed-time graphs of normalized speed/time traces were generated by calculating the median of all speeds at defined 0.1 s intervals after the start of PMF disruption.

Speed histograms for step size analysis were constructed with 1 Hz bins. Multiple Gaussian curves were fit to histogram peaks with mean, SD and amplitude set as free parameters.

For estimation of the stator binding constant, a Chung-Kennedy-Smith filter (Smith, 1998) was used to determine intermediate step size during motor resurrection, with a minimum window size of eight data points and significance rating of 0.05.

Mean spot intensity was calculated by subtracting gross motor spot intensity (at the centre of rotation for tethered cells) from background intensities calculated individually for each cell. Motor spots were defined as described in (Leake *et al*., 2006). Membrane fluorescence background data were calculated by taking the mean fluorescence intensity for each cell (in azide-treated cells), or fluorescence intensity outside defined regions of interest corresponding to motor spots (for untreated cells).

All errors quoted and error bars shown are ± SD.

Acknowledgements

We thank Jan Liphardt for providing pR variant SAR86. M. J. T., N. J. D., B. C. S., R. M. B. and J. P. A. were supported by the Biotechnology and Biological Sciences Research Council (UK).

References

Armitage, J.P., and Evans, M.C.W. (1985) Control of the protonmotive force in *Rhodopseudomonas sphaeroides* in the light and dark and its effect on the initiation of flagellar rotation. *Biochim Biophys Acta* **806:** 42–55.

Béjà, O., Aravind, L., Koonin, E.V., Suzuki, M.T., Hadd, A., Nguyen, L.P., *et al.* (2000) Bacterial rhodopsin: evidence for a new type of phototrophy in the sea. *Science* **289:** 1902–1906.

Blair, D.F., and Berg, H.C. (1988) Restoration of torque in defective flagellar motors. *Science* **242:** 1678–1681.

Block, S.M., and Berg, H.C. (1984) Successive incorporation of force-generating units in the bacterial rotary motor. *Nature* **309:** 470–472.

Braun, T.F., Poulson, S., Gully, J.B., Empey, J.C., Van Way, S., Putnam, A., and Blair, D.F. (1999) Function of proline residues of MotA in torque generation by the flagellar motor of *Escherichia coli*. *J Bacteriol* **181:** 3542–3551.

Chernyak, B.V., Dibrov, P.A., Glagolev, A.N., Sherman, M.Y., and Skulachev, V.P. (1983) A novel type of energetics in a marine alkali-tolerant bacterium: $\Delta\mu$-Na-driven motility and sodium cycle. *FEBS Lett* **164:** 38–42.

Delalez, N.J., Wadhams, G.H., Rosser, G., Xue, Q., Brown, M.T., Dobbie, I.M., *et al.* (2010) Signal-dependent turnover of the bacterial flagellar switch protein FliM. *Proc Natl Acad Sci USA* **107:** 11347–11351.

Fukuoka, H., Wada, T., Kojima, S., Ishijima, A., and Homma, M. (2009) Sodium-dependent dynamic assembly of membrane complexes in sodium-driven flagellar motors. *Mol Microbiol* **71:** 825–835.

Fung, D.C., and Berg, H.C. (1995) Powering the flagellar motor of *Escherichia coli* with an external voltage source. *Nature* **375:** 809–812.

Gabel, C.V., and Berg, H.C. (2003) The speed of the flagellar rotary motor of *Escherichia coli* varies linearly with protonmotive force. *Proc Natl Acad Sci USA* **100:** 8748–8751.

Gittes, F., and Schmidt, C.F. (1998) Interference model for back-focal-plane displacement detection in optical tweezers. *Opt Lett* **23:** 7–9.

Khan, S., Dapice, M., and Reese, T.S. (1988) Effects of *mot* gene expression on the structure of the flagellar motor. *J Mol Biol* **202:** 575–584.

Kobayashi, H., Maeda, M., and Anraku, Y. (1977) Membrane-bound adenosine triphosphatase of *Escherichia coli*. *J Biochem* **81:** 1071–1077.

Kojima, S., and Blair, D.F. (2003) Solubilization and purification of the MotA/MotB complex of *Escherichia coli*. *Biochemistry* **43:** 26–34.

Kojima, S., Imada, K., Sakuma, M., Sudo, Y., Kojima, C., Minamino, T., *et al.* (2009) Stator assembly and activation mechanism of the flagellar motor by the periplasmic region of MotB. *Mol Microbiol* **73:** 710–718.

Kojima, S., Nonoyama, N., Takekawa, N., Fukuoka, H., and Homma, M. (2011) Mutations targeting the C-terminal domain of FliG can disrupt motor assembly in the Na^+-driven flagella of *Vibrio alginolyticus*. *J Mol Biol* **414:** 62–74.

Kuwajima, G. (1988) Construction of a minimum-size functional flagellin of *Escherichia coli*. *J Bacteriol* **170:** 3305–3309.

Leake, M.C., Chandler, J.H., Wadhams, G.H., Bai, F., Berry, R.M., and Armitage, J.P. (2006) Stoichiometry and turnover in single, functioning membrane protein complexes. *Nature* **443:** 355–358.

Leake, M.C., Greene, N.P., Godun, R.M., Granjon, T., Buchanan, G., Chen, S., *et al*. (2008) Variable stoichiometry of the TatA component of the twin-arginine protein transport system observed by in vivo single-molecule imaging. *Proc Natl Acad Sci USA* **105:** 15376–15381.

Li, N., Kojima, S., and Homma, M. (2011) Characterization of the periplasmic region of PomB, a Na^+-driven flagellar stator protein in *Vibrio alginolyticus*. *J Bacteriol* **193:** 3773–3784.

Lo, C.-J., Leake, M.C., Pilizota, T., and Berry, R.M. (2007) Nonequivalence of membrane voltage and ion-gradient as driving forces for the bacterial flagellar motor at low load. *Biophys J* **93:** 294–302.

Macnab, R.M. (2003) How bacteria assemble flagella. *Annu Rev Microbiol* **57:** 77–100.

Manson, M.D., Tedesco, P., Berg, H.C., Harold, F.M., and Van der Drift, C. (1977) A protonmotive force drives bacterial flagella. *Proc Natl Acad Sci USA* **74:** 3060–3064.

Morimoto, Y.V., Nakamura, S., Kami-ike, N., Namba, K., and Minamino, T. (2010) Charged residues in the cytoplasmic loop of MotA are required for stator assembly into the bacterial flagellar motor. *Mol Microbiol* **78:** 1117–1129.

Parkinson, J.S. (1978) Complementation analysis and deletion mapping of *Escherichia coli* mutants defective in chemotaxis. *J Bacteriol* **135:** 45–53.

Philippe, N., Alcaraz, J., Coursange, E., Geiselmann, J., and Schneider, D. (2004) Improvement of pCVD442, a suicide plasmid for gene allele exchange in bacteria. *Plasmid* **51:** 246–255.

Reid, S.W., Leake, M.C., Chandler, J.H., Lo, C.-J., Armitage, J.P., and Berry, R.M. (2006) The maximum number of torque-generating units in the flagellar motor of *Escherichia coli* is at least 11. *Proc Natl Acad Sci USA* **103:** 8066–8071.

Rowe, A.D., Leake, M.C., Morgan, H., and Berry, R.M. (2003) Rapid rotation of micron and submicron dielectric particles measured using optical tweezers. *J Mod Opt* **50:** 1539–1554.

Ryu, W.S., Berry, R.M., and Berg, H.C. (2000) Torque-generating units of the flagellar motor of *Escherichia coli* have a high duty ratio. *Nature* **403:** 444–447.

Sabehi, G., Massana, R., Bielawski, J.P., Rosenberg, M., DeLong, E.F., and Béjà, O. (2003) Novel proteorhodopsin variants from the Mediterranean and Red Seas. *Environ Microbiol* **5:** 842–849.

Sharp, L.L., Zhou, J., and Blair, D.F. (1995) Tryptophan-scanning mutagenesis of MotB, an integral membrane protein essential for flagellar rotation in *Escherichia coli*. *Biochemistry* **34:** 9166–9171.

Smith D.A. (1998) A quantitative method for the detection of edges in noisy time-series. *Philos Trans R Soc Lond B Biol Sci* **353:** 1969–1981.

Sowa, Y., Hotta, H., Homma, M., and Ishijima, A. (2003) Torque-speed relationship of the Na^+-driven flagellar motor of *Vibrio alginolyticus*. *J Mol Biol* **327:** 1043–1051.

Sowa, Y., Rowe, A.D., Leake, M.C., Yakushi, T., Homma, M., Ishijima, A., and Berry, R.M. (2005) Direct observation of steps in rotation of the bacterial flagellar motor. *Nature* **437:** 916–919.

Walter, J.M., Greenfield, D., Bustamante, C., and Liphardt, J. (2007) Light-powering *Escherichia coli* with proteorhodopsin. *Proc Natl Acad Sci USA* **104:** 2408–2412.

Yonekura, K., Maki-Yonekura, S., and Homma, M. (2011) Structure of the flagellar motor protein complex PomAB: implications for the torque-generating conformation. *J Bacteriol* **193:** 3863–3870.

Yuan, J., Branch, R.W., Hosu, B.G., and Berg, H.C. (2012) Adaptation at the output of the chemotaxis signalling pathway. *Nature* **484:** 233–236.

Zhou, J., Lloyd, S.A., and Blair, D.F. (1998) Electrostatic interactions between rotor and stator in the bacterial flagellar motor. *Proc Natl Acad Sci USA* **95:** 6436–6441.

Supporting information

Additional supporting information may be found in the online version of this article.